Supporting Information

High–efficiency photocatalytic reduction of Cr(VI) by Z–scheme electron transfer in UiO-66-NH_2@HDU-25 heterojunctions

Test S1. Characterizations

The morphological features of the materials surface were observed by transmission electron microscopy (TEM, JEOL F200) and scanning electron microscopy (SEM, ZEISS sigma500) and energy-dispersive spectroscopy (EDS) mapping images (EDS spectrometer attached to the TEM). The structures of the samples were examined by X-ray diffraction (XRD, SmartLab SE). X-ray photoelectron spectra (XPS) were collected on an X-ray photoelectron spectrometer (Thermo SCIENTIFIC ESCALAB Xi+). Fourier transform infrared (FT-IR) spectra of the samples were recorded using an infrared spectrometer (Shimadzu IRT racer-100). Samples were analyzed thermogravimetrically (TGA, STA 2500) over a temperature range of 25 to 800 °C with a 10 °C min^{-1} increasing rate. The Brunauer–Emmett–Teller (BET) surface areas and pore volumes were obtained using the N_2 adsorption/desorption technique (TriStar II 3020). The UV–vis diffuse reflectance spectra (DRS, Shimadzu UV-2700) were obtained by the $BaSO_4$ as a reflectance standard at room temperature. The UV–vis absorption spectra are obtained by UV2355 spectrophotometer (Unico UV2355). All the photoelectrochemical tests were performed on an electrochemical workstation (Chenhua CHI E660) with a standard three-electrode system. Electron spin resonance (ESR) signals were recorded with a Bruker ESR A300 spectrometer. The zeta potential of the samples was determined by a zeta potential analyzer (Zetasizer Nano ZSE). The photocatalytic chamber (CEL-LB70) and the xenon light source system (CEL-HXF300-T3) were provided by CEAULIGHT.

In order to obtain a more reasonable structure and reduce the computational cost of the larger model, the HDU-25 structure was optimized by using the B97-3C[1] level

and SMD[2] implicit water solvent model by ORCA[3]software. In order to maintain the planar structure of the HDU-25 structure in isolation, the skeleton atoms were frozen. UiO-66-NH_2 was then extracted from the crystal structure and spliced with the optimized HDU-25 molecule. Finally, CP2K[4,5] software was used to optimize the structure of the splice at the GFN1-Xtb[6] level, in which only the atoms connected between UiO-66-NH_2 and HDU-25 and all the H atoms were relaxed. Based on the optimized final structure, the first 50 electronic excited singlet states were calculated at the TD-CAM-B3LYP[7]-D3(BJ)[8,9]/def2-SVP[10,11] calculation level. The hole-electron excited state analysis[12] and InterFragment Charge Transfer (IFCT) were performed by Multiwfn[13] software. The cub file generated based on Multiwfn was visualized, and the image was rendered by VMD[14] software.

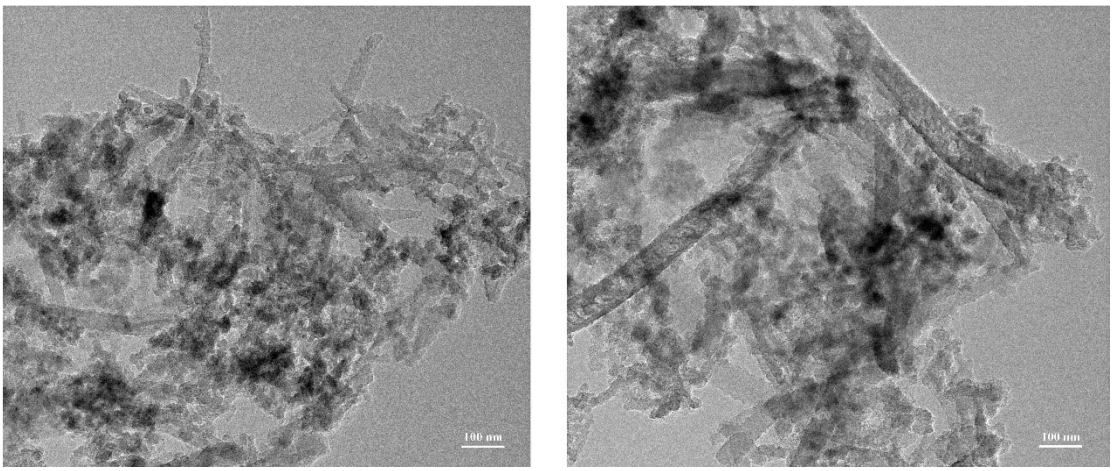

Fig. S1. TEM images of UiO-66-NH_2@HDU-25 (0.5:1)

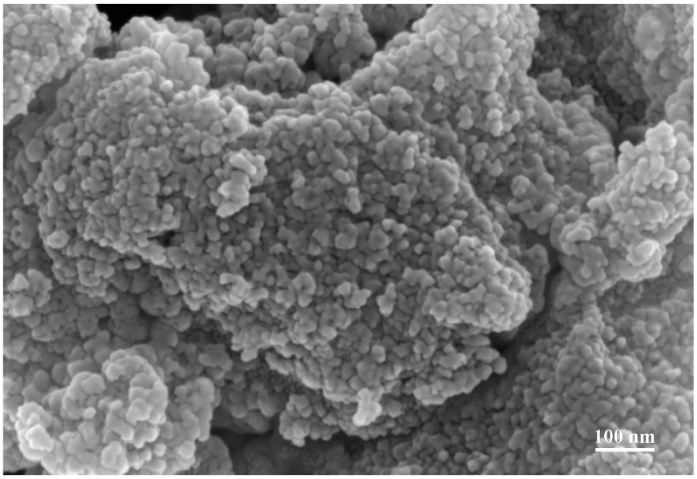

Fig. S2. SEM image of UiO-66-NH_2@HDU-25 (8:1)

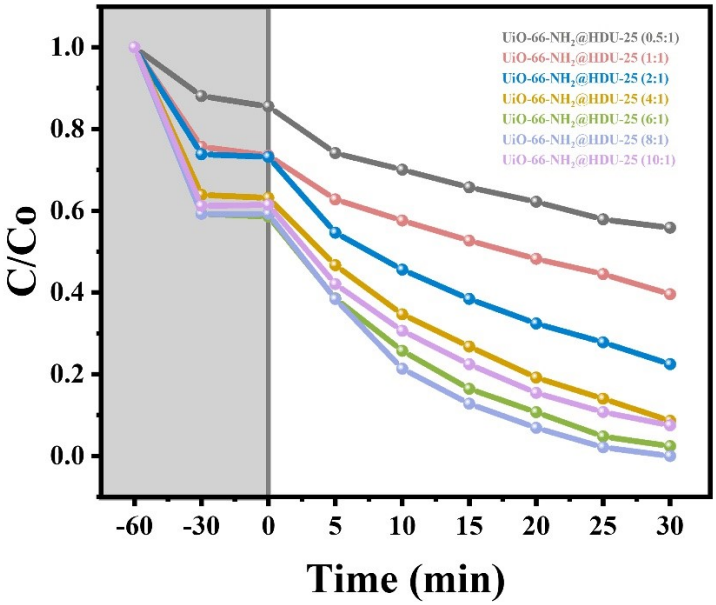

Fig. S3. Photocatalytic effect of a series of UiO-66-NH_2@HDU-25 hybrid materials with different UiO-66-NH_2 mass contents.

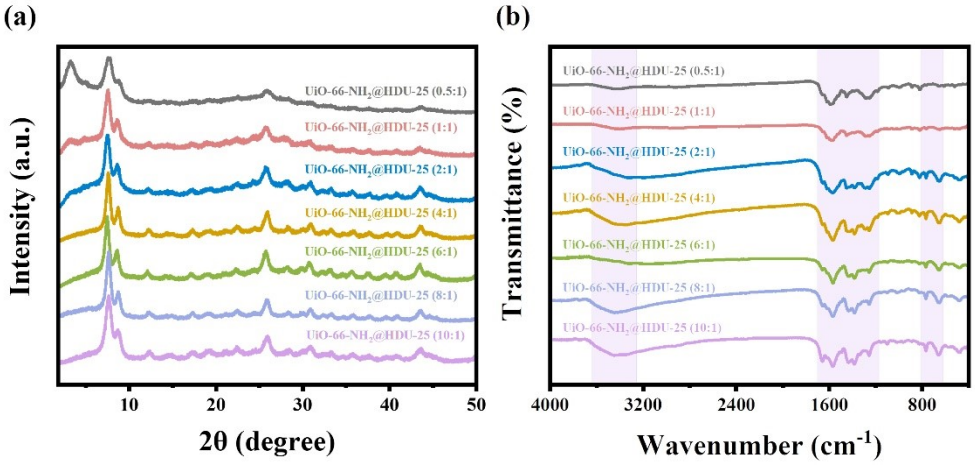

Fig. S4. (a) XRD patterns, (b) FTIR spectra of a series of UiO-66-NH_2@HDU-25 hybrid materials.

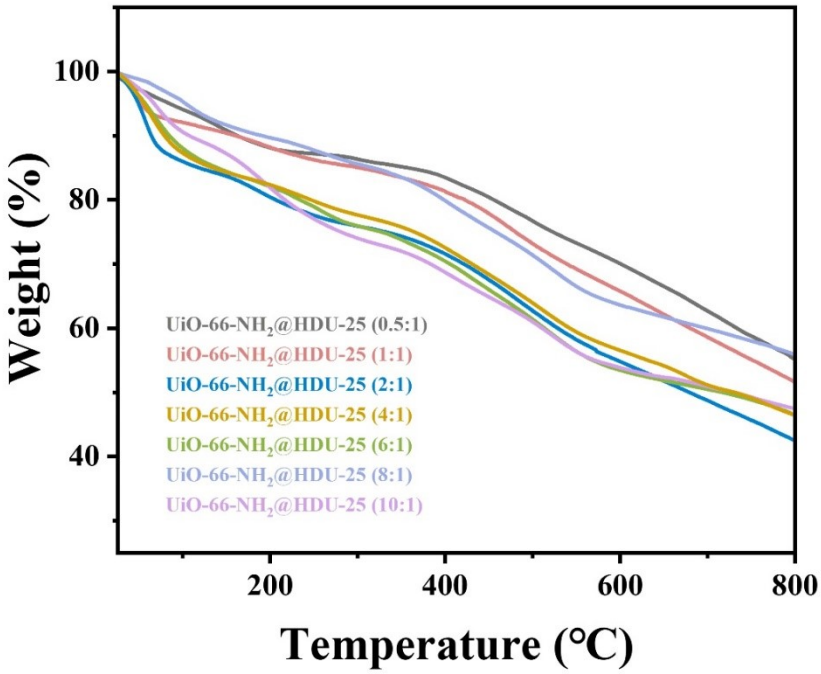

Fig. S5. TG curves of a series of UiO-66-NH_2@HDU-25 hybrid materials.

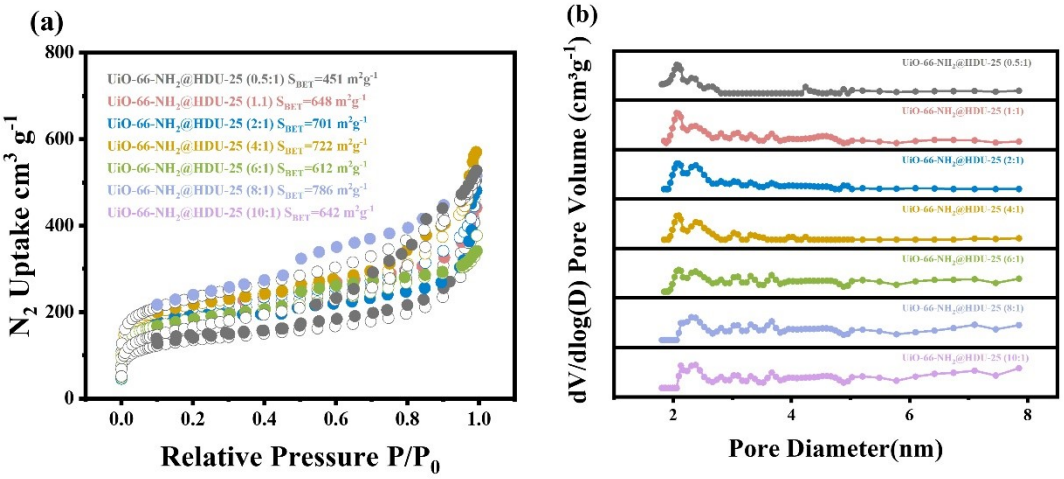

Fig. S6. (a) N_2 adsorption–desorption isotherms, (b) pore size distributions of a series of UiO-66-NH_2@HDU-25 hybrid materials.

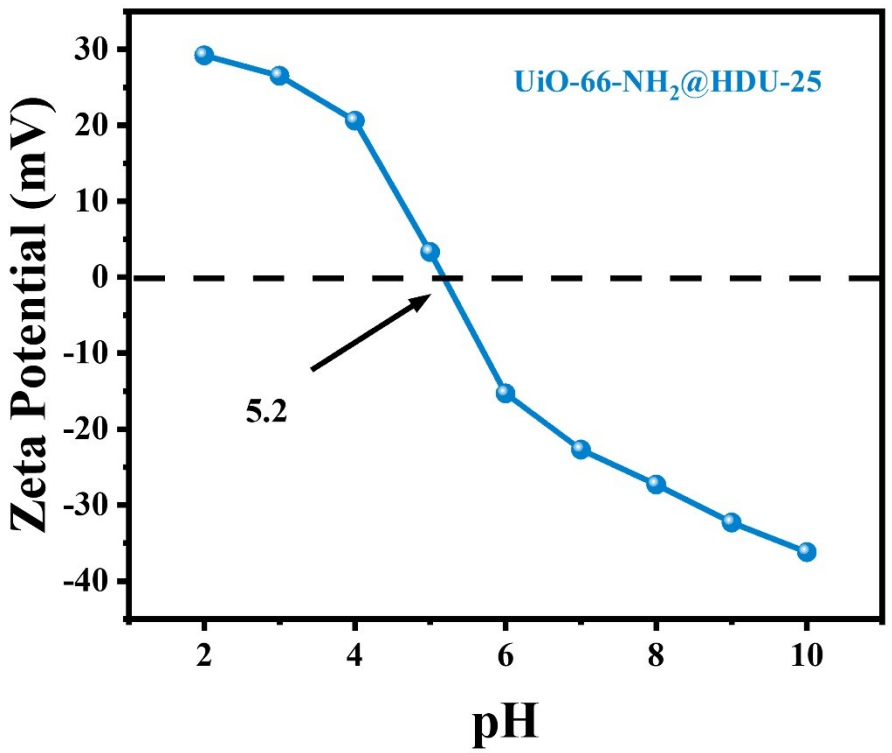

Fig. S7. Zeta potential of UiO-66-NH_2@HDU-25 at different pH values.

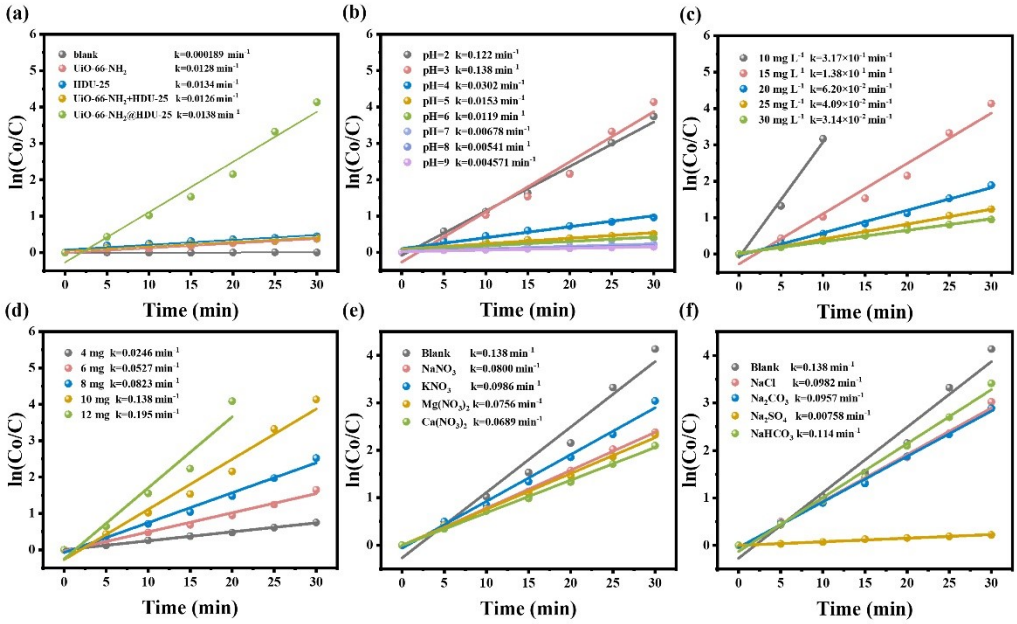

Fig. S8. (a-f) Pseudo-first-order kinetics curves of the photocatalytic Cr(VI) reduction reaction under different conditions.

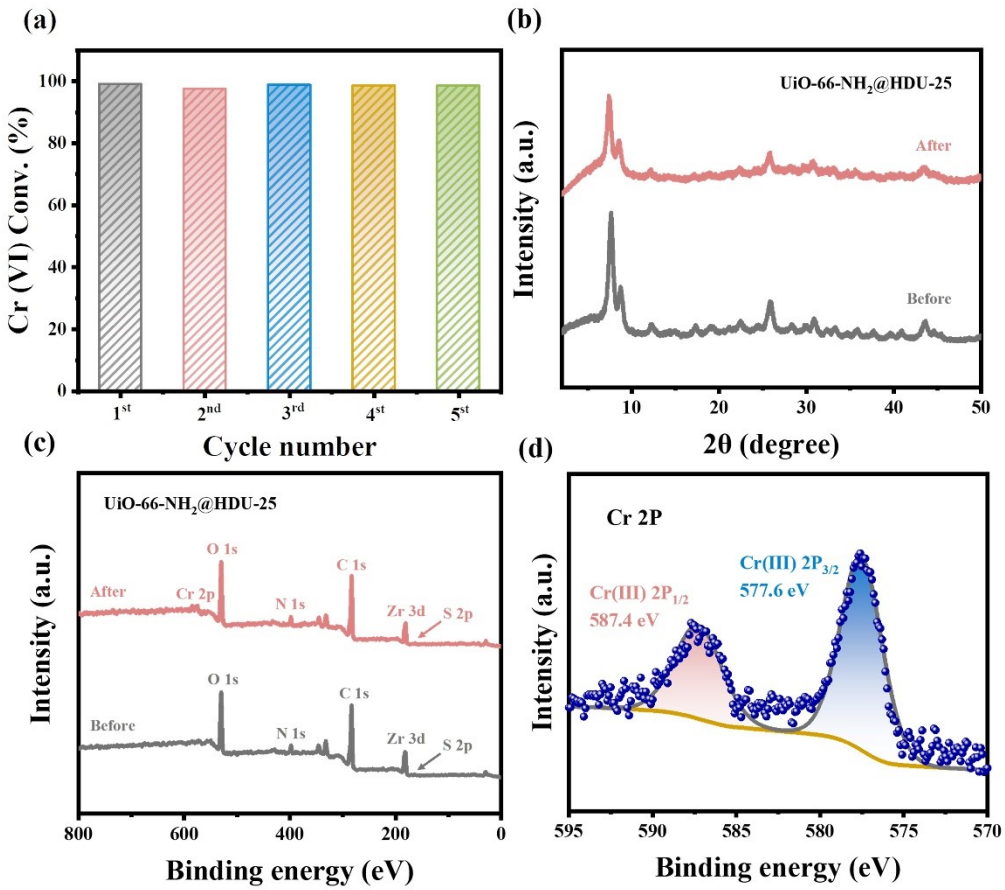

Fig. S9. (a) Cycling performance of UiO-66-NH_2@HDU-25. (b) XRD patterns, and (c) the full XPS spectra of UiO-66-NH_2@HDU-25 before and after cycling. (d) Cr 2p spectra after cycling.

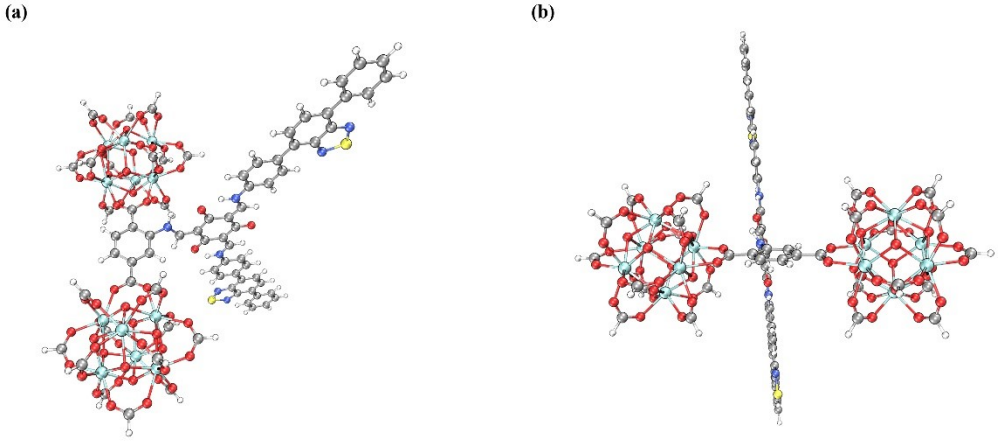

Fig. S10. (a and b) Partial structural modelling of UiO-66-NH_2@HDU-25.

Sample types	Specific surface area (m^2 g^{-1})
UiO-66-NH_2@HDU-25 (0.5:1)	451
UiO-66-NH_2@HDU-25 (1:1)	648
UiO-66-NH_2@HDU-25 (2:1)	701
UiO-66-NH_2@HDU-25 (4:1)	722
UiO-66-NH_2@HDU-25 (6:1)	612
UiO-66-NH_2@HDU-25 (8:1)	786
UiO-66-NH_2@HDU-25 (10:1)	642

Table S1 Specific surface area of a series of UiO-66-NH_2@HDU-25 hybrid materials

References

1 J. G. Brandenburg, C. Bannwarth, A. Hansen and S. Grimme, *J. Chem. Phys.*, 2018, **148**, 064104.

2 A. V. Marenich, C. J. Cramer and D. G. Truhlar, *J. Phys. Chem. B.*, 2009, **113**, 6378-6396.

3 F. Neese, *Wires. Comput. Mol. Sci.*, 2022, **12**, e1606.

4 J. Hutter, M. Iannuzzi, F. Schiffmann and J. VandeVondele, *Wires. Comput. Mol. Sci.*, 2014, **4**, 15-25.

5 T. D. Kühne, M. Iannuzzi, M. Del Ben, V. V. Rybkin, P. Seewald, F. Stein, T. Laino, R. Z. Khaliullin, O. Schütt, F. Schiffmann, D. Golze, J. Wilhelm, S. Chulkov, M. H. Bani-Hashemian, V. Weber, U. Borstnik, M. Taillefumier, A. S. Jakobovits, A. Lazzaro, H. Pabst, T. Müller, R. Schade, M. Guidon, S. Andermatt, N. Holmberg, G. K. Schenter, A. Hehn, A. Bussy, F. Belleflamme, G. Tabacchi, A. Glöss, M. Lass, I. Bethune, C. J. Mundy, C. Plessl, M. Watkins, J. VandeVondele, M. Krack and J. Hutter, *J. Chem. Phys.*, 2020, **152**, 194103.

6 S. Grimme, C. Bannwarth and P. Shushkov, *J. Chem. Theory. Comput.*, 2017, **13**, 1989-2009.

7 T. Yanai, D. P. Tew and N. C. Handy, *Chem. Phys. Lett.*, 2004, **393**, 51-57.

8 S. Grimme, *Wires. Comput. Mol. Sci.*, 2011, **1**, 211-228.

9 S. Grimme, S. Ehrlich and L. Goerigk, *J. Comput. Chem.*, 2011, **32**, 1456-1465.

10 F. Weigend and R. Ahlrichs, *Phys. Chem. Chem. Phys.*, 2005, **7**, 3297-3305.

11 F. Weigend, *Phys. Chem. Chem. Phys.*, 2006, **8**, 1057-1065.

12 Z. Y. Liu, T. Lu and Q. X. Chen, *Carbon*, 2020, **165**, 461-467.

13 T. Lu and F. W. Chen, *J. Comput. Chem.*, 2012, **33**, 580-592.

14 W. Humphrey, A. Dalke and K. Schulten, *Journal of Molecular Graphics*, 1996, **14**, 33-38.